

Structural disparities between chalcedony and macrocrystalline quartz

PETER J. HEANEY

Department of Geological and Geophysical Sciences, Princeton University, Princeton, New Jersey 08544, U.S.A.

DAVID R. VEBLEN

Department of Earth and Planetary Sciences, The Johns Hopkins University, Baltimore, Maryland 21218, U.S.A.

JEFFREY E. POST

Department of Mineral Sciences, NHB 119, Smithsonian Institution, Washington, DC 20560, U.S.A.

ABSTRACT

Examination of length-fast chalcedony by transmission electron microscopy reveals significant structural differences between microcrystalline fibrous quartz and ideal α quartz. Individual crystals that make up chalcedony fibers are elongate along [110] and are twisted about the fiber axis. Streaks in electron diffraction patterns of single fibers indicate pervasive disorder among the {101} and possibly the {011} planes, and in dark-field images the texture of this structural disorder appears dendritic. Because the streak systems associated with {101} and with {011} intersect at the expected locations of primary diffractions associated with the mineral "moganite", demonstrations of the presence of "moganite" require complementary characterization techniques, such as X-ray powder diffraction. In addition, genuine superperiodicities of three, four, and five times the primary translations in quartz are discerned through electron diffraction of chalcedony crystals, and violations of systematic absences associated with the 3_1 screw symmetry are apparent in X-ray diffraction experiments.

INTRODUCTION

That significant structural differences distinguish chalcedony from bulk quartz has been known for well over a century. The lower refractive index and lower density of fibrous quartz led Fuchs (1834) and others to propose that chalcedony is an intimate mixture of crystalline and amorphous quartz. Michel-Lévy and Munier-Chalmas (1892) noted that, in contrast to prismatic quartz, fibrous quartz frequently is elongate in a direction that is normal to the optic axis and displays biaxial behavior, with $2V$ ranging up to 30° . Furthermore, chalcedony fibers systematically twist about the fiber axis (Lacroix, 1900; Bernauer, 1927; Frondel, 1978), and chalcedony is more soluble in H_2O than is quartz (Pelto, 1956; Fournier and Rowe, 1966).

Nevertheless, early X-ray diffraction studies of chalcedony revealed the presence of only pure α quartz (Washburn and Navias, 1922), and the differences between fibrous and prismatic quartz soon were overshadowed by their apparent structural identity. The discovery by SEM of multiple bubble cavities interspersed among the fibers (Folk and Weaver, 1952) further added to the conviction that chalcedonic quartz differs from drusy varieties only in terms of grain size; the presence of molecular H_2O in micropores could account for the lower density and refractive index, as well as the light scattering observed in chalcedony (Pelto, 1956).

Only recently have the differences in the physical prop-

erties of chalcedony and bulk quartz regained the attention of crystallographers. Experiments by Frondel (1982, 1985) and Flörke and his associates (Graetsch et al, 1985; Flörke et al, 1991) have highlighted once again the subtle distinctions between microcrystalline fibrous quartz and macrocrystalline quartz. In this paper, we expand upon these earlier studies, using transmission electron microscopy and X-ray powder diffraction techniques.

EXPERIMENTAL PROCEDURES

Experiments were performed on clear seam-filling chalcedony nodules and on agates that were colorless and translucent. Specimens examined are listed in Table 1. Despite the wide geographic distribution of the agates examined, all samples exhibited similar microstructures and diffraction characteristics. For TEM examination, specimens were sectioned both parallel and perpendicular to the radial quartz fibers at a thickness of $\sim 30 \mu m$ and thinned further by Ar ion milling. Thin foils then were coated lightly with amorphous C. Electron microscopy was performed with a Philips 420 microscope equipped with T or ST objective lenses and operated at 120 keV. X-ray analyses in the TEM were obtained with an EDAX energy-dispersive spectrometer (EDS) and a Princeton Gamma-Tech System IV analyzer.

For X-ray powder diffraction experiments, samples were ground in porcelain mortars under acetone and smeared onto low-background quartz plates or pressed into pack

TABLE 1. Specimens used in this study

Locality	Ident. no.	Source
Mojave Desert, CA	87415	U.S. National Museum
Yellowstone Nat'l Park	83871	U.S. National Museum
Brazil	117434	U.S. National Museum
Mexico	C6537	U.S. National Museum
Australia	131877	U.S. National Museum
Hillsborough Bay, FL	47899	U.S. National Museum
Locality unknown	HAR C	Harvard Mineralogical Museum

mounts. The data were obtained on a Scintag computer-automated powder diffractometer with $\text{CuK}\alpha$ radiation and an intrinsic-Ge solid-state detector. Counting times ranged from 2 to 10 s per 0.03° step for the 2θ range $3\text{--}80^\circ$. A pack mount of specimen 47899 was scanned from 12.2 to $12.3^\circ 2\theta$ ($\lambda = 1.15 \text{ \AA}$) using doubly monochromatized synchrotron radiation at Beamline X7A, Brookhaven National Laboratory.

RESULTS

Absence of opal

Despite past assertions that the quartz in chalcedony is intergrown with opal (Correns and Nagelschmidt, 1933; Donnay, 1936; Jones 1952), careful X-ray powder diffraction studies of chalcedony (e.g., Novák, 1947; Midgley, 1951) have revealed little in the way of opaline phases. Graetsch et al. (1985) reported fibrous opal-C within the thin rims surrounding agate nodules from the Rio Grande do Sul in Brazil, and powder neutron diffraction experiments of chalcedony from the silicified corals of Hillsborough Bay, Florida, revealed a minor amorphous silica component (Heaney and Post, unpublished manuscript). Nevertheless, in the course of our TEM examination, we observed no opaline silica residing either between or within chalcedony fibers. Rather, chalcedony fibers were uniformly crystalline and tightly packed.

Optical characterization of fibers

As observed with the petrographic microscope, all the fibrous quartz analyzed during these experiments was length-fast, indicating elongation normal to *c*. Thin sections of the various specimens displayed textures that are typical for chalcedony (see Frondel, 1962): sheafs of fibers emanated from a few points along the rims of the nodules, suggesting initial precipitation at discrete nucleation centers. Optical examination indicated that a strong orientational relationship exists among the fibers that make up these sheafs. The fibers within the bundles went to extinction simultaneously (Fig. 1), and the extinction bands that result from twisting of the optic *c* axis about the fiber axis (Runzelbänderung) were fairly continuous across fiber bundle boundaries (Fig. 2).

Despite the optical indications of crystallographic continuity within these sheafs, selected-area electron diffraction (SAED) of regions within the fiber bundles produced ring patterns (Fig. 3), especially in fine-grained areas. All Debye-Scherrer rings were present, and they remained

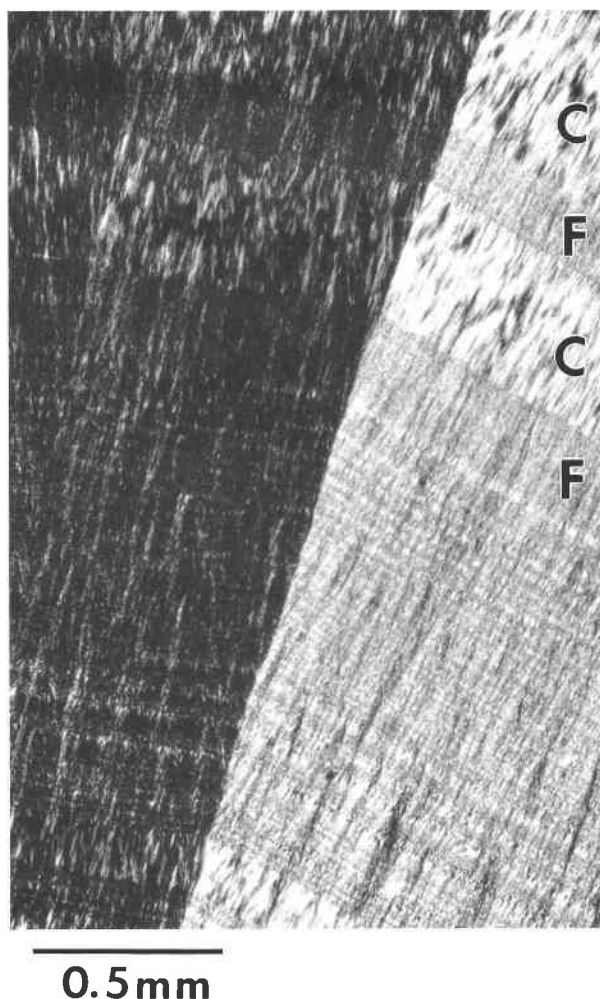


Fig. 1. Optical micrograph of chalcedony. Fibers contained within the same bundle go to extinction simultaneously. Coarse fibers (C) are distinguished from fine-grained areas (F) by longer twist periodicity, higher birefringence, and absence of fine banding.

visible as the specimen was rotated 90° about the goniometer axis. Such electron diffraction effects indicate a fairly random orientation of the crystallites that constitute the fibers, as is consistent with observations made by Sunagawa and Ohta (1976). In these fine-grained regions, crystals appeared equant and measured $<0.1\text{--}0.5 \mu\text{m}$ across. Preferred orientation among these crystals was discernible only when the diffracting area was limited to $<5 \mu\text{m}$ in diameter. As was noted also by Mische et al. (1984), grains that do share a common crystallographic orientation appear to be aligned (Fig. 4). Presumably, these strings of crystallites make up the fine-grained fibers that are observed in the optical microscope.

In many chalcedony specimens, these zones of fine-grained quartz fibers alternate with bands of coarse fibers. In some instances, this banding is highly periodic (Wang and Merino, 1990), but frequently the distance between

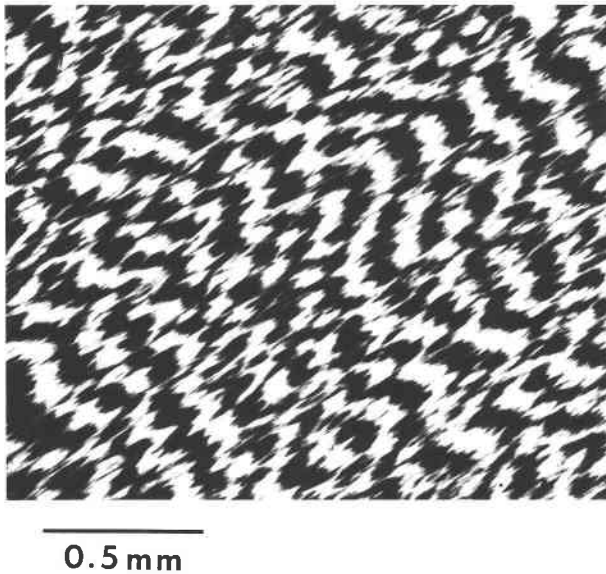


Fig. 2. Extinction bands in fibrous quartz are periodic along the fiber length and roughly continuous across fiber boundaries. This chevron extinction pattern is characteristic of chalcedony and results from the cooperative rotation of the optic axes about the fiber axes along the lengths of the fibers.

coarse-grained bands oscillates randomly. Optical examination of thick petrographic sections ($\sim 100 \mu\text{m}$) reveals that these coarser-grained areas have a distinctly higher birefringence than the finer-grained regions. The fibers in the coarse-grained zones can exceed $2 \mu\text{m}$ in diameter and $5 \mu\text{m}$ in length, and the fibrous morphology is evident even in bright-field images (Fig. 5).

Fiber orientation and twisting

Numerous X-ray diffraction studies have demonstrated that chalcedony fibers are elongate primarily along $[110]$ and more rarely along $[2\bar{1}0]$ (see Frondel, 1962). In addition, a SAED pattern superimposed upon the image of a coarse chalcedony fiber in Figure 5 confirms the $[110]$ orientation of these crystals. The growth of chalcedony fibers normal to the c axis differs from the behavior of prismatic quartz, which typically is elongate parallel to c .

Also in contrast to bulk quartz, chalcedony fibers usually are twisted about the $[110]$ fiber axis, giving rise to Runzelbänderung, as mentioned above. Our TEM examination of chalcedony revealed that this twisting occurs within individual crystals that constitute the fibers; it does not appear to arise from rotational misalignment of multiple single crystals along the fiber direction. In one experiment, a traverse was performed along the length of a single crystal within a coarse fiber whose axis of elongation was parallel to the goniometer axis. Consequently, the pitch of the fiber twisting could be ascertained by monitoring the relative orientations of major zone axes along the length of the crystal. This analysis placed the helicoid periodicity at about $550 \mu\text{m}$ per twist, though from optical observation this periodicity clearly is quite

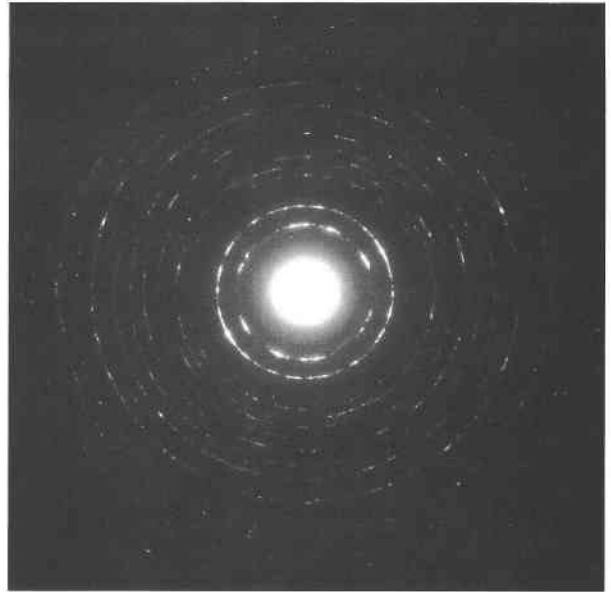


Fig. 3. A SAED pattern from an area of fine-grained fibrous quartz about $10 \mu\text{m}$ in diameter. Although some preferred orientation of the fibers is discernible, the overall ringlike quality of the pattern suggests that orientations of the quartz crystals are poorly correlated within regions of this size.

variable. Frondel (1978) cited a range for the twist period of 20–300 cm.

Several explanations have been offered to explain fiber twisting in chalcedony. Graetsch et al. (1987) asserted that rotation about the fiber axis arises from lattice misfit between quartz-like modules and moganite-like modules in chalcedony. (Note: the name “moganite” has not been accepted by the IMA CNMMN.) Wang and Merino (1990) proposed that trace substitutions of Al for Si distort the lattice and induce a helical habit. By analogy with the growth mechanisms operative in some whisker crystals, Frondel (1978) attributed chalcedony twisting to screw dislocations in which the Burgers vectors are parallel to the direction of elongation. More specifically, Heaney (1993) observed that a spiral growth mechanism activated by screw dislocations with Burgers vectors equal to $n/2[110]$ accounts not only for fiber twisting but also for the pervasive planar disorder that characterizes chalcedony.

Planar disorder within fibrous quartz

Intersecting streak systems. SAED patterns of chalcedony commonly reveal complex streak systems. These streaks are particularly evident in diffraction patterns with zone axes parallel to $\langle \bar{1}21 \rangle$ (Figs. 6 and 7) and $\langle \bar{1}\bar{1}1 \rangle$ (Fig. 8). In their TEM study of Brazilian agates, Mieke et al. (1984) noted that these streaks occur along the $\langle 101 \rangle^*$ directions, indicating extensive planar disorder parallel to $\{101\}$. On the basis of the orientation of these composition surfaces, they postulated that the disorder arises

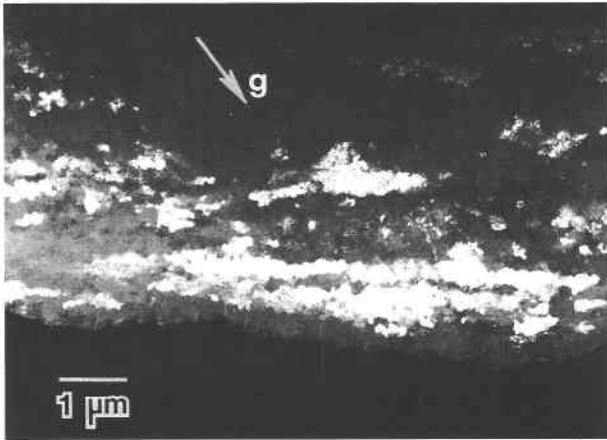


Fig. 4. A dark-field image ($g = 100$) of fine-grained agatoid quartz reveals that crystals with similar orientations form a linear arrangement. These crystals are separated by low-angle grain boundaries, and presumably they make up the fibers observed with the optical microscope.

from random interstratification of Brazil twin lamellae. In addition, Mieke et al. (1984) attributed apparent superlattice diffractions at multiples of $\frac{1}{3}\langle 012 \rangle^*$ (as seen in Fig. 6) to intersections within the $\langle 101 \rangle^*$ streak system. The three individuals that make up this streak system (Fig. 9) are the vectors $\langle 101 \rangle^*$, $\langle \bar{1}11 \rangle^*$, and $\langle 01\bar{1} \rangle^*$. The intersections of $\langle 01\bar{1} \rangle^*$ with the reciprocal space plane defined by the vectors $\langle 101 \rangle^*$ and $\langle \bar{1}11 \rangle^*$ occur at multiples of $\frac{1}{3}\langle 012 \rangle^*$. Therefore, the extra spots seen in Figure 6 along the direction $\langle 012 \rangle^*$ may represent the out of plane $\langle 01\bar{1} \rangle^*$ streak. Similarly, we commonly observed apparent superlattice diffractions at multiples of $\frac{1}{2}\langle 011 \rangle^*$ (Fig. 8A), and these extra spots may arise from the intersection of the $\langle 01\bar{1} \rangle^*$ streak, with the reciprocal space plane defined by $\langle 101 \rangle^*$ and $\langle \bar{1}10 \rangle^*$.

Presence of moganite. The SAED patterns also reveal intensity maxima at $h \pm \frac{1}{2}$, k , $l \pm \frac{1}{2}$ (Fig. 7). Mieke et al. (1984) attributed these superlattice diffractions to regions in which the left- and right-handed twin lamellae alternate uniformly at the scale of the unit cell, thereby doubling the primary translations along c and a_1 . The rigorous alternation along $\{101\}$ of slices of left- and right-handed quartz creates the distinct silica polymorph called moganite, which was first observed as seams in ignimbrite flows in Gran Canaria (Flörke et al., 1976, 1984). Electron diffraction patterns of moganite exhibit no streaking along the $\langle 101 \rangle^*$ directions, and the $h \pm \frac{1}{2}$, k , $l \pm \frac{1}{2}$ reflections are quite sharp. Mieke and Graetsch (1992) offered a structure solution for moganite with space group symmetry $I2/a$, based on X-ray powder diffraction experiments.

Graetsch et al. (1987) interpreted chalcedony as a kind of structural hybrid between quartz and moganite. With-in some regions, a chalcedony fiber may contain quartz lamellae that are entirely left- or right-handed, and in other areas, lamellae of opposite chirality may oscillate

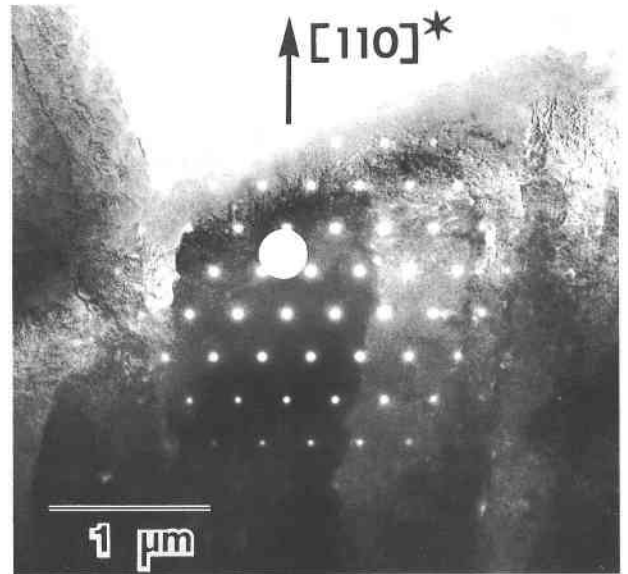


Fig. 5. The chalcedony fibers in this bright-field image of coarse-grained chalcedony are oriented vertically. Superposition of a SAED pattern taken from the white circular region onto the image of the fibers confirms that the direction of elongation is $[110]^*$, which is parallel to $[110]$.

with strict periodicity, thereby giving rise to moganite. However, the bulk of a typical chalcedony fiber consists of a highly aperiodic alternation of twin lamellae, producing highly concentrated planar defects. These defect

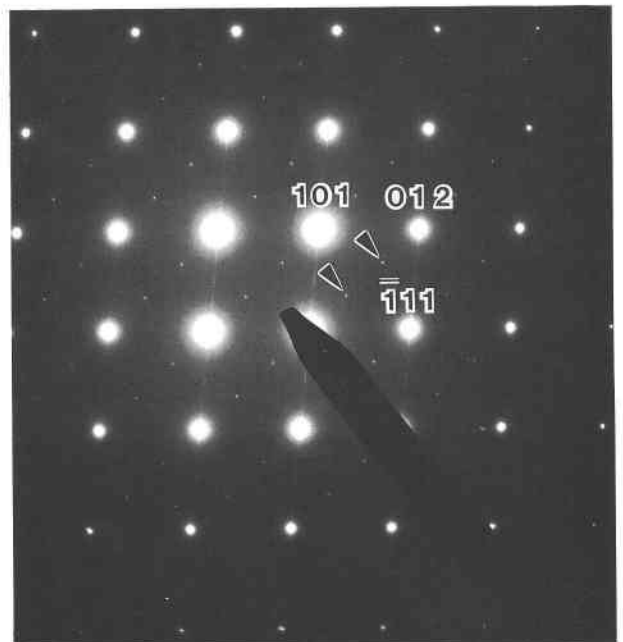


Fig. 6. SAED pattern with zone axis $\langle \bar{1}21 \rangle$ reveals streaking along $\langle 101 \rangle^*$. Apparent superlattice reflections occur at positions corresponding to multiples of $\frac{1}{3}\langle 012 \rangle^*$ (arrows), and they arise from intersections within the single $\langle 101 \rangle^*$ streak system.

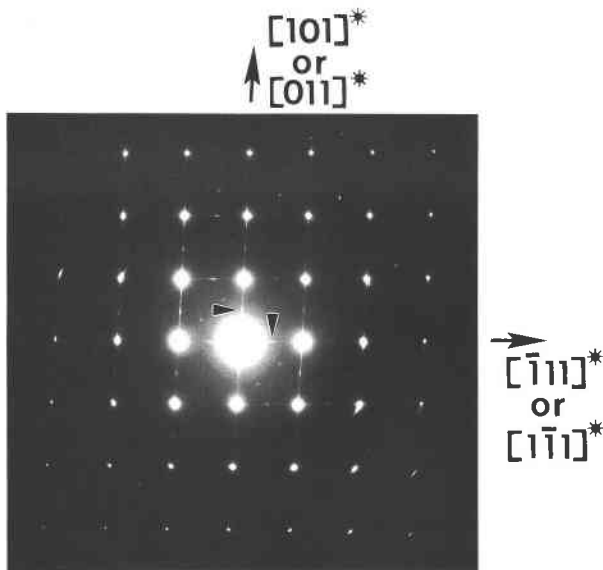


Fig. 7. A SAED pattern with zone axis $\langle \bar{1}21 \rangle^*$ exhibits streaks along symmetrically equivalent $[101]^*$ and $[\bar{1}\bar{1}]^*$ directions or $[011]^*$ and $[1\bar{1}]^*$ directions. Distinguishing between these two possibilities requires knowledge of the kinematic intensities of the diffraction spots. Additional moganite-like superlattice spots are shown with arrows.

structures are not restricted to fibrous microcrystalline silica; Wenk et al. (1988) described similar features in sedimentary chert and fine-grained quartz from the slickenside surface of a granite.

Ambiguities in moganite identification. Our SAED studies (Figs. 6, 7, 8) of both agatoid and seam-filling chalcedony clearly revealed the existence of the planar disorder observed by Mische et al. (1984). In dark-field images of the coarse fibers, these defects appear as featherlike or dendritic textures: traces of the planar defects run parallel to the fiber direction along the fiber cores, and additional defect traces branch out from these central cores (Fig. 10). The distance between the traces of the planar defects is somewhat variable, but the spacings typically range from 50 to 100 Å. The featherlike texture of these chalcedony fibers strikingly resembles the chevron pattern created by the intergrown laths of nearly pure moganite (Heaney and Post, 1992), perhaps indicating that the crystallographic constraints that dictate the habit of end-member moganite also are operative during the growth of chalcedony.

Although we concur with Graetsch et al. (1987) that most chalcedony contains a disordered mixture of quartz and moganite, our investigations suggest that electron diffraction cannot reveal without ambiguity the presence of moganite in association with planar disorder. The space group for α quartz is $P3_121$ (or $P3_221$). Although the quartz structure has only threefold rotational symmetry along the c axis, the lattice for the trigonal crystal system contains a sixfold symmetry operator along c . Thus, as with all trigonal crystals, the point group symmetry of the

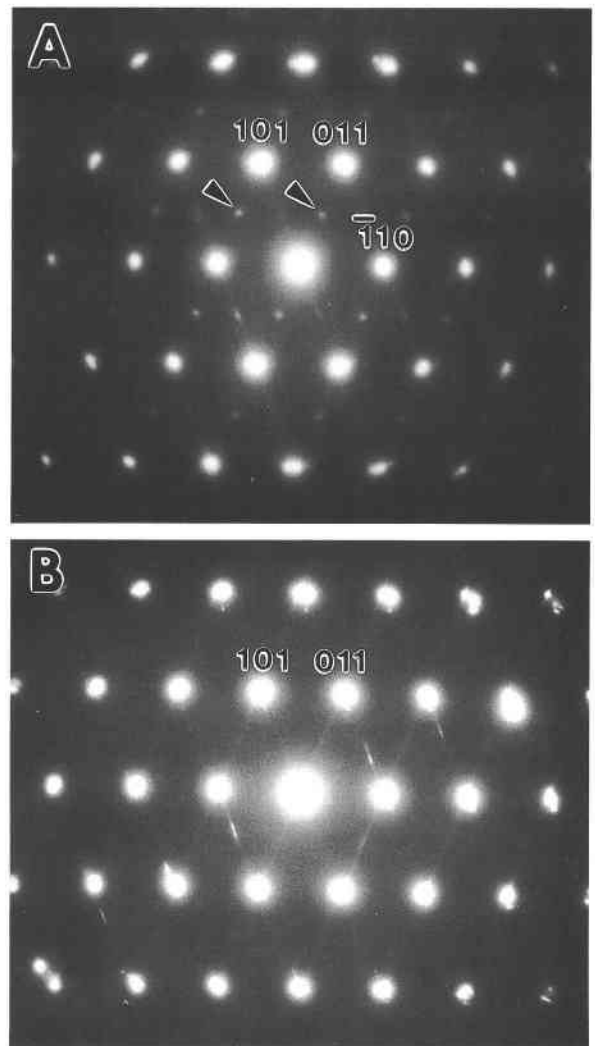


Fig. 8. SAED patterns with zone axis $\langle \bar{1}\bar{1}1 \rangle^*$. (A) Faint streaking is observed along $\langle 101 \rangle^*$, and apparent superlattice reflections (arrows) occur at positions that correspond to multiples of $\frac{1}{2}\langle 011 \rangle^*$. (B) Streaks are visible along both the $\langle 101 \rangle^*$ and the $\langle 011 \rangle^*$ directions.

quartz lattice is higher than that of the quartz structure. As a result, diffraction patterns with zone axes that are related by a sixfold rotation around c appear geometrically identical, but the intensities of corresponding spots differ. Diffraction patterns of quartz from zones other than $[001]$ or $[uv0]$ cannot be indexed unambiguously in the absence of intensity data, and intensities from electron diffraction are unreliable because of dynamical scattering processes.

Consequently, determination of the streak systems observed in the SAED patterns of chalcedony is problematic. Although the streaks observed in our diffraction patterns could be indexed to the $\langle 101 \rangle^*$ direction, as was done by Mische et al. (1984), those streaks could as easily be indexed to the $\langle 011 \rangle^*$ direction (Fig. 7). This ambiguity in reciprocal space translates to an uncertainty in

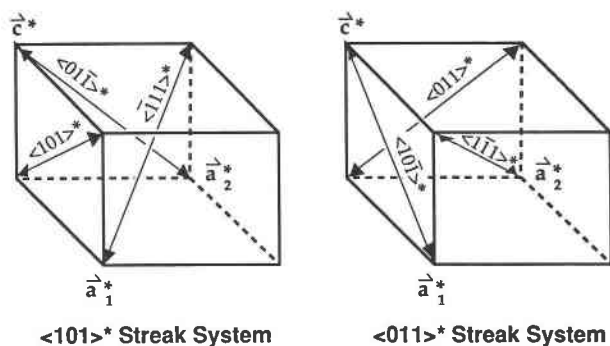


Fig. 9. A schematic diagram of the symmetrically distinct $\langle 101 \rangle^*$ (left) and $\langle 011 \rangle^*$ (right) streak systems in fibrous quartz. Superposition of these streak systems leads to intersections at $h \pm 1/2$, k , $l \pm 1/2$; h , $k \pm 1/2$, $l \pm 1/2$; and $h \pm 1/2$, $k \pm 1/2$, $l \pm 1/2$.

real space regarding the planes that actually are disordered. The defects may occur parallel to $\{101\}$ or to $\{011\}$ or to both sets of planes.

This distinction is significant. In Figure 9, the $\langle 101 \rangle^*$ and the $\langle 011 \rangle^*$ streak systems are mapped out in separate reciprocal-space unit cells. If planar defects occur among both the $\{101\}$ and the $\{011\}$ planes, these two streak systems are excited simultaneously. When the $\langle 101 \rangle^*$ streak system is superimposed upon the $\langle 011 \rangle^*$ streak system, the streaks intersect at several points: $h \pm 1/2$, k , $l \pm 1/2$; h , $k \pm 1/2$, $l \pm 1/2$; and $h \pm 1/2$, $k \pm 1/2$, $l \pm 1/2$. The intersections of these streaks appear in electron diffraction patterns as points of heightened intensity. Consequently, they may mask genuine superlattice spots, or they may be mistaken for genuine superlattice spots. Because the positions occupied by the intersections of the $\langle 101 \rangle^*$ and the $\langle 011 \rangle^*$ streak systems are exactly those occupied by the superlattice spots produced by moganite, the presence of those diffraction maxima may not always indicate the presence of moganite.

McLaren and Pitkethly (1982) have correctly pointed out that structural constraints favor an orientation for Brazil twin boundaries along $\{101\}$; this composition plane requires the least amount of distortion from the ideal quartz structure at the interface. Nevertheless, structural continuity also can be maintained across Brazil composition planes oriented parallel to $\{011\}$. Indeed, Frondel (1962) observed that Brazil twin lamellae in amethysts typically occur parallel either to $\{101\}$ and $\{011\}$. Under the conditions of rapid nonequilibrium crystallization that characterize the growth of chalcedony fibers (Wang and Merino, 1990), the formation of Brazil composition planes parallel to the less favorable $\{011\}$ orientation may not be uncommon.

Our own experiments suggest that in some cases the apparent superlattice reflections at $h \pm 1/2$, k , $l \pm 1/2$ and related points can indeed arise from intersections of the $\langle 101 \rangle^*$ and the $\langle 011 \rangle^*$ streak systems. In Figure 8B, streaks along both the $\langle 101 \rangle^*$ and the $\langle 011 \rangle^*$ directions are clearly observable. In addition, the intensity maxima

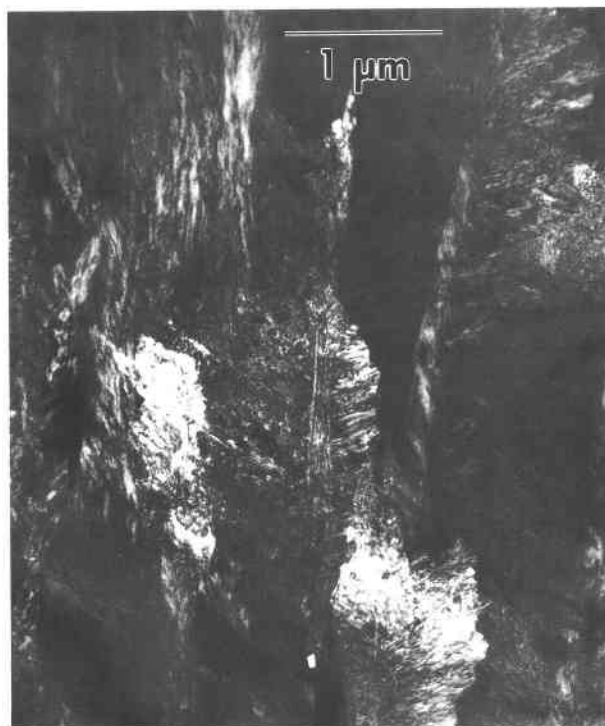


Fig. 10. Dark-field image ($g = 101$) of agate fibers reveals the pervasive planar defects that give the crystals a featherlike appearance.

of the $h \pm 1/2$, k , $l \pm 1/2$ spots typically are elongate and somewhat diffuse, in contrast to the sharp intensities associated with the true superlattice diffractions described below. Furthermore, Rietveld refinement of X-ray diffraction patterns produced by most of the chalcedony analyzed in this study revealed relatively low concentrations of moganite, usually < 15 wt%, as is typical for agates (Heaney and Post, 1992). Nevertheless, the $h \pm 1/2$, k , $l \pm 1/2$ diffraction maxima consistently appeared even in electron diffraction patterns from coarse chalcedony fibers, which contained much less moganite (< 5 wt%) than the fine-grained regions. Consequently, we argue that identification of moganite in chalcedony cannot rely on TEM evidence alone and should be supplemented by X-ray powder diffraction techniques.

Superstructures in fibrous quartz

In addition to the intensity maxima that result from the intersection of $\langle 101 \rangle^*$ and $\langle 011 \rangle^*$ streaks, we detected faint but distinct diffraction spots along various reciprocal lattice directions between the primary spots. These superlattice spots include: $1/3$ 021, $1/4$ $\bar{1}$ 41, and $1/5$ 032 (Fig. 11A–11C), and they correspond to multiples of the primary translations of α quartz (e.g., three, four, and five times). A doubled superperiodicity, as found in moganite (Miehe et al., 1984), may occur as well, but the intersecting streaks prevent a definitive determination.

Several lines of evidence suggest that these superlattice

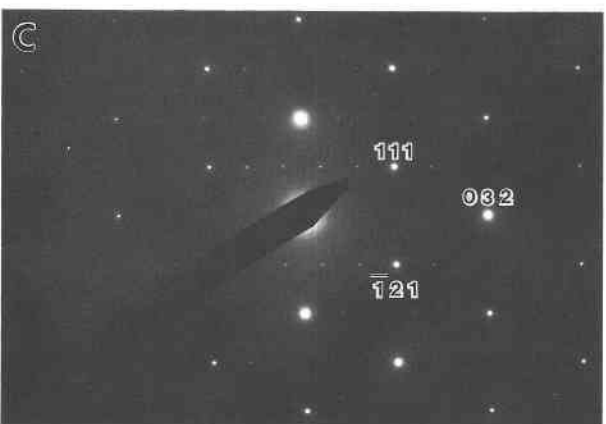
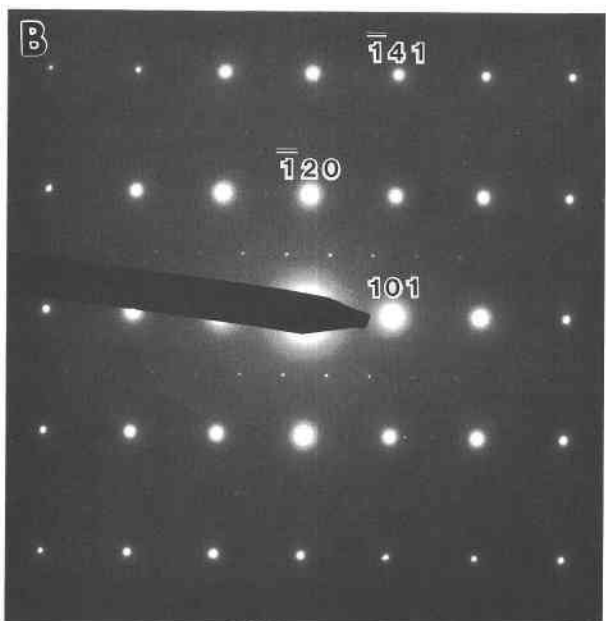
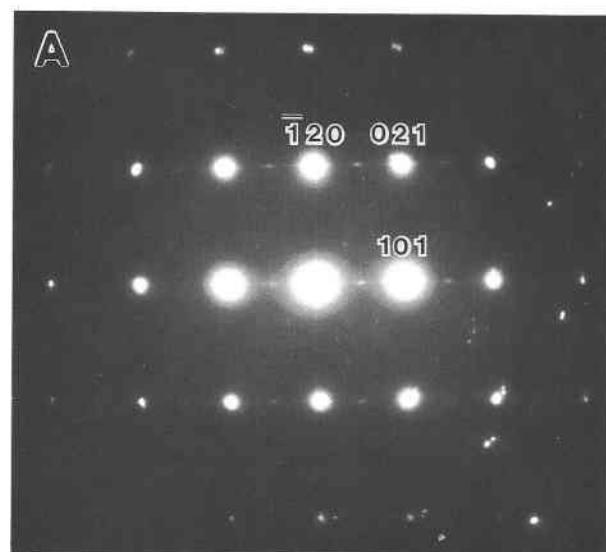


Fig. 11. Genuine superlattice diffractions in chalcedony. Extra spots occur at (A) $\frac{1}{2}$ 021; (B) $\frac{1}{4}$ $\bar{1}41$, and (C) $\frac{1}{2}$ 032.

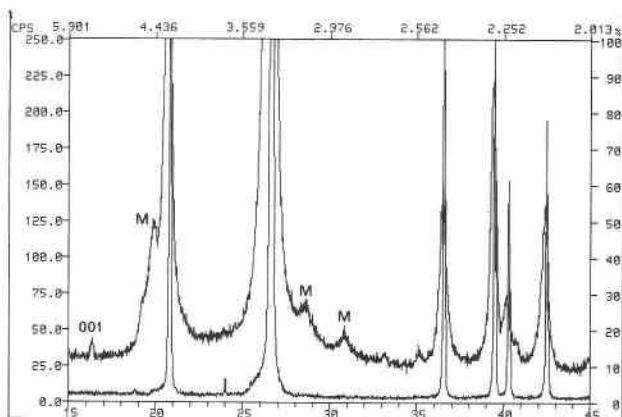


Fig. 12. Enlarged X-ray powder diffraction pattern of chalcedony (top) and prismatic quartz (bottom). Peaks labeled M are produced by intergrown moganite. The peak at $16.3^\circ 2\theta$ corresponds to the (001) d value for quartz and violates the threefold screw symmetry. The top scale is given in ångströms, the bottom scale in 2θ (degrees).

spots did not arise from intersecting streaks. The superlattice spots were circular, sharp, and of lesser intensity than the streak intersections. No streak systems other than $\langle 101 \rangle^*$ and $\langle 011 \rangle^*$ were discerned during our electron diffraction work, and it appears that these would not give rise to the extra diffraction spots observed. Lastly, electron diffraction patterns with the same zone axis but from different chalcedony crystals exhibited different superperiodicities. Specifically, the SAED patterns in Figure 11A and 11B have the same zone axis, $[2\bar{1}2]$, but they exhibit different superlattice maxima. No superlattice diffraction peaks were evident in the X-ray powder diffraction patterns taken for these samples, suggesting that the intensities of the extra spots in electron diffraction patterns are strongly enhanced by dynamical diffraction.

Violation of threefold screw symmetry

The 3_1 or 3_2 screw axes that characterize macrocrystalline quartz require systematic absences among $00l$ reflections for which $l \neq 3n$. These absences are commonly violated in electron diffraction patterns of prismatic quartz because of dynamical scattering processes, but they are obeyed in single-crystal and powder X-ray diffraction patterns. However, powder X-ray diffraction patterns of chalcedony did reveal weak intensities for values of 2θ that correspond to the prohibited 001 reflection (Fig. 12). This peak typically displayed intensities that were three to four times that of the background, and its full width at half-maximum (FWHM) was approximately $0.2^\circ 2\theta$ with $\text{CuK}\alpha$ radiation.

That this symmetry violation is not spurious is supported by several observations: (1) Although d_{002} of moganite corresponds to $\sim 5.4 \text{ \AA}$, samples of nearly pure moganite from Gran Canaria did not reveal this peak, presumably because the structure factor associated with this reflection in moganite is very low. In addition, the

peak could be discerned in weathered chert samples that, according to Rietveld refinement, contain no moganite. (2) The $K\beta$ peak for the (100) planes of quartz is expected to occur in the vicinity of this reflection. However, a synchrotron X-ray radiation scan over this area also revealed the peak, and the synchrotron radiation used in this experiment was highly monochromatic. (3) Although it was of low intensity, this peak was observed in scores of diffraction patterns from fibrous and nonfibrous microcrystalline silica specimens in the collection of the U.S. National Museum of Natural History.

The consistent violation of the threefold screw operation indicates that the space group symmetry for chalcedony is not trigonal but either monoclinic or triclinic.

DISCUSSION

This study underscores one primary conclusion: chalcedony is not simply fine-grained quartz. In one sense, this knowledge extends back to prehistoric times, when hunter-gatherers spurned coarsely crystalline quartz in favor of microcrystalline cherts and chalcedonies for fashioning their tools; the densely interwoven chalcedony fibers lent a toughness to this material that is not matched by prismatic quartz. Differences in the chemical properties of chalcedony and quartz also have been recognized by manufacturers of concrete; whereas quartz crystals can serve as relatively inert components of a concrete mix, chalcedony is highly reactive and induces mechanical failure (Bean and Tregoning, 1944).

Nevertheless, these differences and the optical discrepancies between chalcedony and quartz were submerged under the prodigious weight of X-ray powder diffraction evidence early in this century. The nearly identical powder patterns produced by quartz and chalcedony reveal much about their structural disparity: it must involve changes of such subtlety that they are apparently not detectable by conventional X-ray diffraction techniques. One common culprit in such circumstances is structural H, and much evidence suggests that H is incorporated into the structure of chalcedony. Flörke et al. (1982) determined that agates contain from 1 to 2 wt% H_2O , which is divided more or less equally between interstitial molecular H_2O and silanole-group water (SiOH). On the basis of infrared spectroscopy studies of chalcedony, Graetsch et al. (1987) estimated that one-third of the silanole is surficial and the remaining two-thirds is internal.

We speculate that the true superperiodicities and the violation of the threefold screw symmetry observed in chalcedony arise from structural H. Simulated X-ray powder diffraction patterns for quartz in a triclinic setting indicate that the appearance of a 001 peak can be induced by displacement of a single O atom by $\sim 0.2 \text{ \AA}$ along the z direction. Bonding H atoms may be responsible for such anionic displacements. Moreover, the superlattice diffractions observed in SAED patterns but not in X-ray patterns also may involve short-range structural distortions due to local ordering of H atoms. These speculations await direct empirical validation.

The fibrosity and planar disorder that distinguish chalcedony from prismatic quartz may provide a window into differences between the mechanisms by which these two silica species crystallize. This possibility is addressed in a separate paper (Heaney, 1993).

ACKNOWLEDGMENTS

Our thanks go to Pete Dunn of the U.S. National Museum, to Carl Francis and Bill Metropolis of the Harvard Mineralogical Museum, to Clifford Frondel, and to Eugene Smelik for providing specimens that were used for this study. Joe Pluth performed the synchrotron data collection. Helpful reviews were provided by Alain Baronnet, Dave Vaniman, and an anonymous reviewer. This research was supported by NSF grants EAR-8609277, EAR-8903630, and EAR-9206031. Electron microscopy was performed in the Johns Hopkins HRTEM laboratory, which was established with partial support from NSF grant EAR-8300365, and the General Motors Electron Microbeam Facility of the Princeton Materials Institute.

REFERENCES CITED

- Bean, L., and Tregoning, L.L. (1944) Reactivity of aggregate constituents in alkaline solutions. *Journal of the American Concrete Institute*, 16, 37–51.
- Bernauer, F. (1927) Über Zickzackbänderung (Runzelbänderung) und verwandte Polarisationserscheinungen an Kristallen und Kristallaggregaten. *Neues Jahrbuch für Mineralogie, Geologie, und Paläontologie Beilageband*, 55, 92–143.
- Correns, C.W., and Nagelschmidt, G. (1933) Über Faserbau und optische Eigenschaften von Chalcedon. *Zeitschrift für Kristallographie*, 85, 199–213.
- Donnay, J.D.H. (1936) La biréfringence de forme dans la calcédoine. *Annales de la Société Géologique de Belgique*, 59, 289–302.
- Flörke, O.W., Jones, J.B., and Schmincke, H.-U. (1976) A new microcrystalline silica from Gran Canaria. *Zeitschrift für Kristallographie*, 143, 156–165.
- Flörke, O.W., Köhler-Herbertz, B., Langer, K., and Tönges, I. (1982) Water in microcrystalline quartz of volcanic origin: Agates. *Contributions to Mineralogy and Petrology*, 80, 324–333.
- Flörke, O.W., Flörke, U., and Giese, U. (1984) Moganite: A new microcrystalline silica-mineral. *Neues Jahrbuch für Mineralogie Abhandlungen*, 149, 325–336.
- Flörke, O.W., Graetsch, H., Martin, B., Röller, K., and Wirth, R. (1991) Nomenclature of micro- and non-crystalline silica minerals, based on structure and microstructure. *Neues Jahrbuch für Mineralogie Abhandlungen*, 163, 19–42.
- Folk, R.L., and Weaver, C.E. (1952) A study of the texture and composition of chert. *American Journal of Science*, 250, 498–510.
- Fournier, R.O., and Rowe, J.J. (1966) Estimation of underground temperatures from the silica content of water from hot springs and wet-steam wells. *American Journal of Science*, 264, 685–697.
- Frondel, C. (1962) *The system of mineralogy*, vol. III, 334 p. Wiley, New York.
- (1978) Characters of quartz fibers. *American Mineralogist*, 63, 17–27.
- (1982) Structural hydroxyl in chalcedony (Type B quartz). *American Mineralogist*, 67, 1248–1257.
- (1985) Systematic compositional zoning in the quartz fibers of agates. *American Mineralogist*, 70, 975–979.
- Fuchs, J.H. (1834) Zum Amorphismus fester Körper. *Annalen der Physik und Chemie*, 31, 577–583.
- Graetsch, H., Flörke, O.W., and Miehé, G. (1985) The nature of water in chalcedony and opal-C from Brazilian agate geodes. *Physics and Chemistry of Minerals*, 12, 300–306.
- (1987) Structural defects in microcrystalline silica. *Physics and Chemistry of Minerals*, 14, 249–257.
- Heaney, P.J. (1993) A proposed mechanism for the growth of chalcedony. *Contributions to Mineralogy and Petrology*, 115, 66–74.
- Heaney, P.J., and Post, J.E. (1992) The widespread distribution of a novel

- silica polymorph in microcrystalline quartz varieties. *Science*, 255, 441–443.
- Jones, F.T. (1952) Iris agate. *American Mineralogist*, 37, 578–587.
- Lacroix, A. (1900) Sur une forme de silice anhydre optiquement négative. *Comptes Rendus de l'Académie des Sciences*, 130, 430–432.
- McLaren, A.C., and Pitkethly, D.R. (1982) The twinning microstructure and growth of amethyst quartz. *Physics and Chemistry of Minerals*, 8, 128–135.
- Michel-Lévy, A., and Munier-Chalmas, C.P.E. (1892) Mémoire sur diverses formes affectées par le réseau élémentaire du quartz. *Bulletin de la Société française de Minéralogie*, 15, 159–190.
- Midgley, H.G. (1951) Chalcedony and flint. *Geological Magazine*, 88, 179–184.
- Miche, G., and Graetsch, H. (1992) Crystal structure of moganite: A new structure type for silica. *European Journal of Mineralogy*, 4, 693–706.
- Miche, G., Graetsch, H., and Flörke, O.W. (1984) Crystal structure and growth fabric of length-fast chalcedony. *Physics and Chemistry of Minerals*, 10, 197–199.
- Novák, J. (1947) Les modifications fibreuses de la silice. *Bulletin de la Société française de Minéralogie*, 70, 288–299.
- Pelto, C.R. (1956) A study of chalcedony. *American Journal of Science*, 254, 32–50.
- Sunagawa, I., and Ohta, E. (1976) Mechanism of formation of chalcedony. *Science Reports of the Tohoku University*, 13, 131–146.
- Wang, Y., and Merino, E. (1990) Self-organizational origin of agates: Banding, fiber twisting, composition, and dynamic crystallization model. *Geochimica et Cosmochimica Acta*, 54, 1627–1638.
- Washburn, E.W., and Navias, L. (1922) The relation of chalcedony to the other forms of silica. *Proceedings of the National Academy of Sciences*, 8, 1–5.
- Wenk, H.-R., Shaffer, S.J., and Van Tendeloo, G. (1988) Planar defects in low temperature quartz. *Physica Status Solidi A*, 107, 799–805.

MANUSCRIPT RECEIVED OCTOBER 12, 1992

MANUSCRIPT ACCEPTED JANUARY 14, 1994